ChemCatChem

Research Article
doi.org/10.1002/cctc.202500615

Chemistry Europe
European Chemical Societies Publishing

www.chemcatchem.org

H_2 Production from Ammonia Borane: Integrating Experiments, Computational Fluid Dynamics, and Statistical Analysis for Predicting and Optimizing Process and Reactor Design

Panayiota Adamou,[a] Eleana Harkou,[a] Silvio Bellomi,[b] Ilaria Barlocco,[b] Dimitris Mintis,[c, d] Antreas Afantitis,[c, d] Juan J. Delgado,[e] Xiaowei Chen,[e] George Manos,[f] Nikolaos Dimitratos,[g, h] Alberto Villa,*[b] and Achilleas Constantinou*[a]

In this study, an iridium catalyst ($Ir/Ni_{10}Ce$) was used for the catalytic hydrolysis of ammonia borane (AB). The parameters tested were temperature, stirring rate, AB concentration, and AB-to-catalyst molar ratio. By integrating a simple Langmuir–Hinshelwood kinetic in a computational fluid dynamics (CFD) simulation, the experimental results were validated with a maximum error of 13% observed at only two experimental conditions, while on the rest it was lower than 10%, showcasing the robustness of the model. In all experimental cases, AB resulted in over 85% H_2 yield. Statistical analysis was also implemented to uncover the effect of the four main factors: temperature, stirring rate, AB concentration, and substrate (AB) to catalyst ratio, on the three response variables: reaction time, TOF, and H_2 yield. Radar plots are also presented, illustrating how two-factor interaction influences the response variables. By combining temperature with either concentration or catalyst amount, a profound effect on the reaction time was observed. The combination of experimental work along with computational work of CFD and statistical analysis can significantly enhance a reaction process by targeting the most impactful factors, allowing experiments with optimized reaction conditions for better results in terms of H_2 yield and catalytic performance. Considering also the interaction of the variables enables further process optimization by focusing on specific parameter combinations without wasting resources.

1. Introduction

The storage of hydrogen (H_2) is an extremely important barrier to overcome for the implementation of a hydrogen-based economy. Its storage in liquid form requires low temperatures, which is not economically viable.[1] Hydrogen storage materials are a great way to store H_2 in a chemical form, where under certain conditions, evolution of H_2 is obtained and the spent storage materials can be recycled and rehydrogenated.[2] Examples of such materials include metal hydrides, chemical hydrides, complex hydrides, liquid organic hydrogen carriers, and so on.

Ammonia borane (NH_3BH_3, AB) is an example of a chemical hydride with a high content of hydrogen (19.6 wt%),[3] which can be released through the process of thermolysis or the process of solvolysis (hydrolysis or methanolysis). The process of thermolysis requires higher reaction temperatures, while solvolysis can be achieved at ambient temperatures, offering a more promising method to generate H_2.[4] The most effective method to

[a] P. Adamou, E. Harkou, A. Constantinou
Department of Chemical Engineering, Cyprus University of Technology, 57 Corner of Athinon and Anexartisias, Limassol 3036, Cyprus
E-mail: a.konstantinou@cut.ac.cy

[b] S. Bellomi, I. Barlocco, A. Villa
Dipartimento di Chimica, Università degli Studi di Milano, via Golgi 19, Milano I-20133, Italy
E-mail: alberto.villa@unimi.it

[c] D. Mintis, A. Afantitis
NovaMechanics Ltd, Nicosia 1070, Cyprus

[d] D. Mintis, A. Afantitis
Entelos Institute, Larnaca 6059, Cyprus

[e] J. J. Delgado, X. Chen
Departamento de Ciencia de los Materiales, Ingeniería Metalúrgica y Química Inorgánica, Facultad de Ciencias, Universidad de Cádiz, Campus Río San Pedro, (Cádiz) E, Puerto Real 11510, Spain

[f] G. Manos
Department of Chemical Engineering, University College London, London WCIE 7JE, UK

[g] N. Dimitratos
Department of Industrial Chemistry "Toso Montanari", Alma Mater Studiorum University of Bologna, Viale Risorgimento 4, Bologna 40136, Italy

[h] N. Dimitratos
Center for Chemical Catalysis-C3, Alma Mater Studiorum University of Bologna, Viale Risorgimento 4, Bologna 40136, Italy

Supporting information for this article is available on the WWW under https://doi.org/10.1002/cctc.202500615

release H_2 seems to be hydrolysis, where, in the presence of a catalyst, AB can undergo hydrolytic dehydrogenation rapidly. Its hydrolytic reaction is presented in Equation (1), where 3 moles of H_2 are released from 1 mole of AB.[5]

$$NH_3BH_3\,(aq.) + 2H_2O\,(l) \rightarrow NH_4^+\,(aq.) + BO_2^-\,(aq.) + 3H_2\,(g) \quad (1)$$

Many studies have investigated the mechanism by which AB is hydrolyzed. The following three steps are believed to be the potential mechanism: (i) formation of activated complex species between the surface of the metal particle and AB molecules, (ii) a H_2O molecule attacks (S_N2 mechanism) causing the dissociation of the B—N bond and (iii) the BH_3 intermediate that resulted from the B—N bond breakage is hydrolyzed, forming H_2 and a BO_2^- ion.[6–8] However, the exact mechanism remains unknown/unclear because it depends on the metal sites of the catalyst.

A thorough understanding of the hydrolysis mechanism, and particularly the rate-determining step, is crucial for the design and development of an effective catalyst. Numerous catalysts have been investigated up to this point for the hydrolysis of AB, including noble metals which result in high catalytic activity and low activation energy.[9–11] A study by Chandra and Xu,[12] demonstrated AB hydrolysis using different catalysts and precursors at ambient temperatures. Transition metals (Pt, Rh, and Pd) exhibited the best performance, releasing rigorously H_2. Among the three transition metals, Pt catalyst achieved the highest catalytic activity. Yao et al.,[13] developed PtPd catalysts for AB hydrolysis. The $Pt_{25}Pd_{75}$ catalyst exhibited a superior catalytic activity attributed to its structure. Pd supported on g-C_3N_4 catalysts were synthesized by Shingole et al.[14] The CNPd5 catalyst exhibited the best performance with calculated activation energy of 27.36 kJ/mol and good reusability after 6 cycles.

However, due to their scarcity and high cost, it is preferred to include non-noble metals or supports, since the synergistic interaction of the two metals or the metal-support will enhance the catalytic activity and lower the development cost of the catalyst.[15] A study by Li et al.,[16] synthesized RuNi bimetallic nanocatalysts supported on graphene-like transition metal carbide via co-reduction of ruthenium chloride and nickel chloride using AB as a reducing agent. The RuNi/$Ti_3C_2X_2$ catalysts were very active for the AB hydrolysis toward H_2 at ambient temperatures. The activation energy was relatively low (25.7 kJ/mol) compared to other studies, and the TOF number had a value of 824.7 mol H_2 (mol Ru.min^{-1}). The effect of other supports, such as TiO_2, Al_2O_3, and MCM-41, was also evaluated and the results revealed that the $Ti_3C_2X_2$ support had the highest initial rate. This was due to the fact that there was a better dispersion and smaller particle size of the Ru/Ni particles in the $Ti_3C_2X_2$ support than the rest of the supports.

A valuable tool for validation of these experimental studies and optimization is computational fluid dynamics (CFD). Coupling kinetic data with modeling, provides the opportunity of validating the experimental results by comparing them with the predicted ones.[17–23] Besides this, CFD tools are able to give detailed flow visualization of a system, offering 2D or 3D representations of the flow behavior, including velocity fields, vortex formation, and pressure distribution.[24,25] CFD modeling, for the catalytic hydrolysis of AB has not yet been implemented.

Statistical analysis is the science of collecting, analyzing, and presenting data to discover trends, relationships, or underlying patterns. Design and statistical analysis of experiments couple two major phases of experimentation since the analysis of the data reflects the design of the experiment.[26] By identifying patterns and validating experimental data, statistical analysis ensures that the results are statistically significant and not random, strengthening their credibility. Moreover, it allows the opportunity to group variables and study their relationship. Since AB hydrolysis is a parameter-dependent reaction, statistical analysis will bring forefront the most significant parameters to achieve 100% conversion, high H_2 yield, and high catalytic activity.

In this study, experimental data on the hydrolysis of AB using an Ir/$Ni_{10}Ce$ catalyst are presented, varying parameters such as temperature, stirring rate, AB concentration, and AB-to-catalyst ratio. CFD studies were also performed to validate the experimental results using a Langmuir-Hinshelwood kinetic model. The usage of a smaller reactor was also tested. Statistical analysis was carried out in order to find the parameters with the most significant contribution to the experimental results, and also two-factor analysis was conducted for the three-response values of reaction time, TOF and H_2 yield to uncover interactions between parameters.

2. Results and Discussion

2.1. Catalyst Characterization

Figure 1 presents a STEM-HAADF image of the Ir/$Ni_{10}Ce$ catalyst. Even though Ni distributes nearly uniformly with Ce, in certain areas some Ni agglomeration is observed (Figure 1c). Ce, Ni, and Ir maps in Figure 1e show that Ir is dispersed across the entire surface of the $NiCeO_x$ support and does not preferentially localize in Ni-rich regions. Figure S1 depicts small and highly homogenous distributed Ir particles in the range from 0.5 to 3 nm with an average particle size calculated at 1.1 nm based on measuring more than 150 Ir nanoparticles.

XRD analysis (Figure S2) confirmed that the metal oxide catalyst exhibited peaks at 2θ values of 28.3, 32.8, 47.0, 55.7, and 58.4 °, which are characteristics of the planes (111), (110), (211), (221), and (220) of the cubic CeO_2 structure.[48] In contrast, no clear reflections of Ni and Ir were detected, probably due to the fact that Ir and Ni are mostly well dispersed into CeO_2 support.

2.2. Catalytic Hydrolysis Tests

The catalytic hydrolysis of AB generates only H_2 and ions, however, under certain conditions ammonia (NH_3) is also formed. Thus, it is important to achieve high H_2 yield by choosing an appropriate catalyst. In our previous study on hydrous hydrazine decomposition, Ir/$Ni_{10}Ce$ catalyst was utilized which exhibited

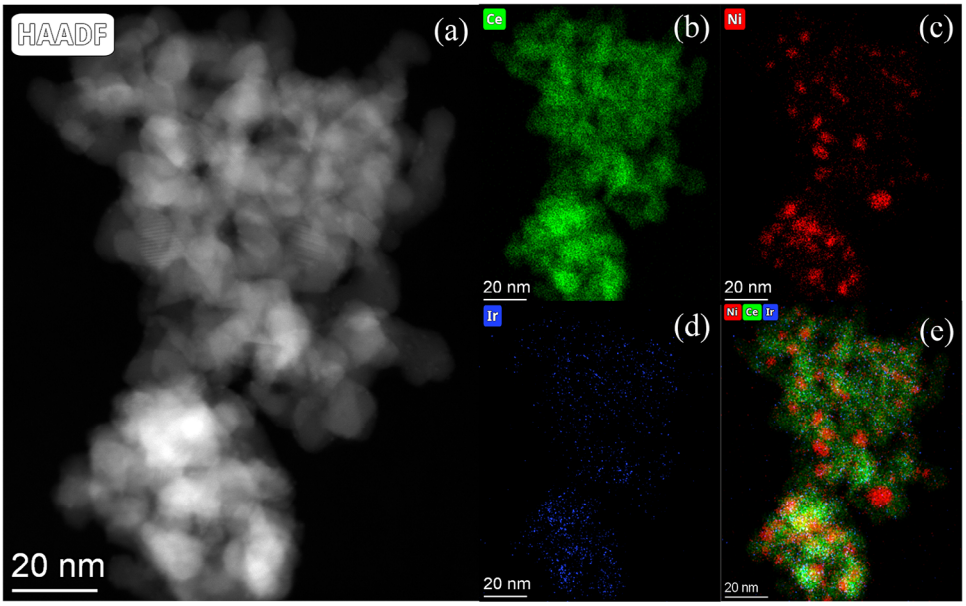

Figure 1. (a) STEM-HAADF image, (b) Ce, (c) Ni, (d) Ir, and (e) Ce, Ni, and Ir maps of Ir/Ni_{10}Ce catalyst.

great results. Therefore, it was chosen for this reaction as well to investigate its performance. In the case of using solely iridium catalysts for AB hydrolysis, there are no data in the literature as we are aware, since only Ir complex catalysts were tested for this reaction.[27–32] In this study, it would be interesting to gain new information in terms of H_2 yield and catalytic activity, testing the Ir/Ni_{10}Ce catalyst.

A series of experiments was conducted varying parameters such as temperature, stirring rate, AB concentration, and catalyst mass that might influence the H_2 yield. Moreover, the effect of the reactor size was investigated. All the experiments were performed in a batch reactor, and the following graphs visualize the ratio of the produced H_2 toward the initial amount of AB. According to the stoichiometry of the reaction (Equation 1), a 100% H_2 yield corresponds to a ratio value of 3. CFD studies were conducted afterwards, using the Langmuir–Hinshelwood kinetics to compare with the experimental data. The CFD model was able to predict the data accurately with maximum error of 13%.

2.3. Temperature Effect

The effect of temperature on AB hydrolysis was firstly investigated. The hydrolysis of AB can be achieved at room temperature, and a typical temperature study range for this reaction is 15–65 °C.[33–36] In general, the rate of the reaction is increased with the reaction temperature based on the Arrhenius formula $k = Ae^{E_a/RT}$. Figure 2 shows the measured moles of H_2 generated per mole of injected AB at three different temperatures (30 °C, 40 °C, and 50 °C). It is evident that by increasing the temperature, the reaction rate is indeed increased, and the reaction time is decreased. It is evident that the CFD model is in good agreement with the experimental results. The TOF value (Figure 3) was doubled when the temperature was increased from 30 °C to 40 °C and then was more than doubled from 40 °C to 50 °C. However,

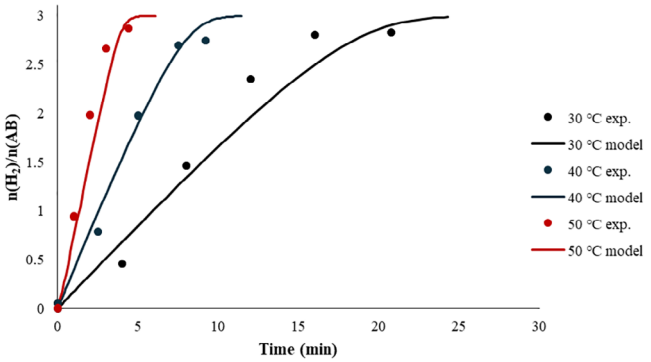

Figure 2. Effect of temperature on AB hydrolysis. Reaction conditions: 0.5 mL of AB in 5 mL water (90.9 mM AB), stirring rate of 1400 rpm, and 3000:1 substrate to metal molar ratio.

H_2 yield was not affected and in all cases, there was over 90% H_2 yield. The activation energy was found 65.9 kJ/mol (Figure S3), lower compared to another study (~100 kJ/mol)[31] using Ir complexes as a catalyst. Activation energy, TOF values, as well as experimental conditions are presented in Table S1 in the supplementary file in comparison with other noble metals that were used as catalysts for this reaction.

2.4. Effect of Stirring Rate

Tests were carried out at stirring rates of 250, 500, 750, and 1400 rpm, in order to determine the most suitable speed at which the hydrolysis reaction would not be limited by diffusion. It is evident from the graph (Figure 4) that above 500 rpm the curves follow the same path, while at 250 rpm the initial rate is slower and also results in less H_2 yield. Observing also the TOF values (Figure 5), it is clear that at 250 rpm the TOF is way lower, while from 500 to 1400 rpm it reaches a plateau. To ensure that

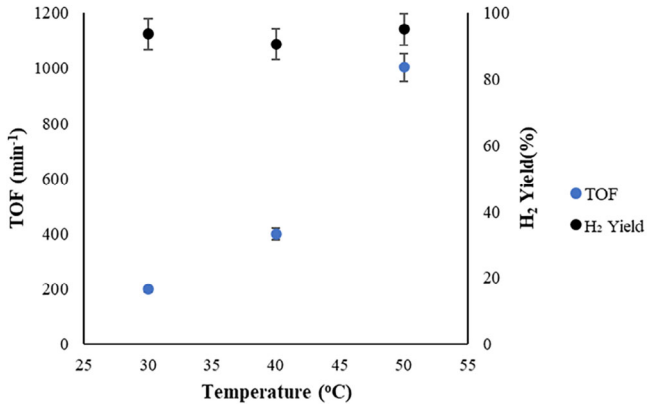

Figure 3. TOF values (left *y*-axis) and H2 yield (right *y*-axis) at temperatures of 30–50 °C.

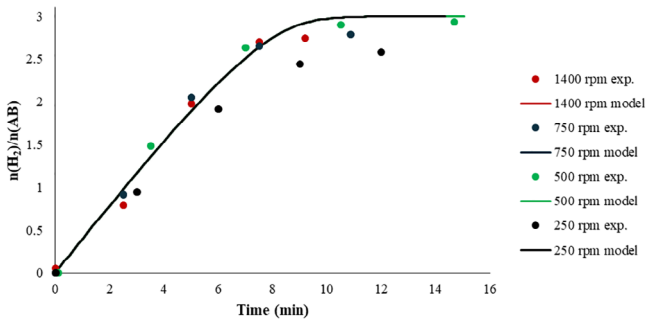

Figure 4. Effect of stirring rate on AB hydrolysis. Reaction conditions: 0.5 mL of AB in 5 mL water (90.9 mM AB), 3000:1 substrate to metal molar ratio, and 40 °C.

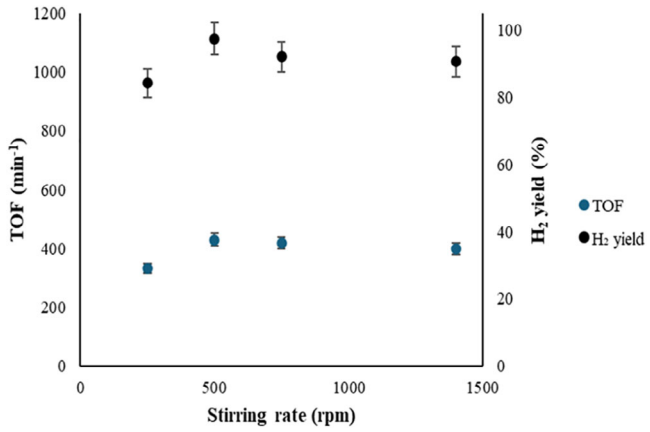

Figure 5. TOF values (left *y*-axis) and H_2 yield (right *y*-axis) at stirring rates of 250–1400 rpm.

there are no external mass transfer limitations, the stirring rate of 1400 rpm was selected as the optimum value. CFD studies agree with the experimental results with a maximum error of 13% at 250 rpm.

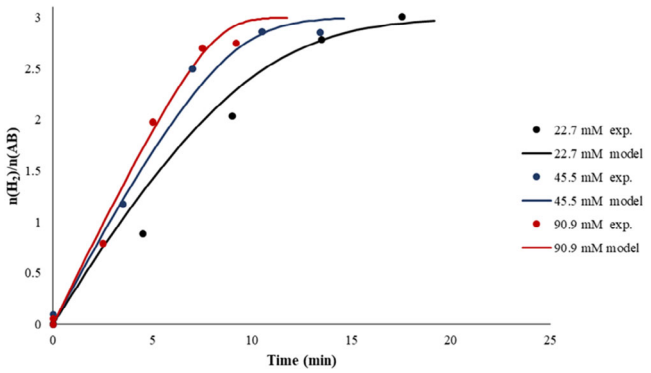

Figure 6. Effect of AB concentration on the hydrolysis of AB. Reaction conditions: stirring rate of 1400 rpm, 3000:1 substrate-to-metal molar ratio, and 40 °C.

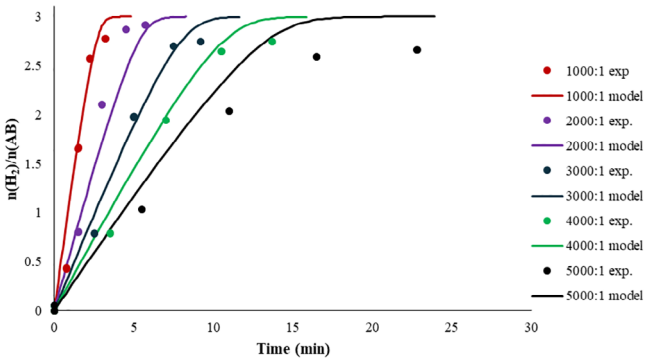

Figure 7. Effect of substrate-to-catalyst ratio on AB hydrolysis. Reaction conditions: 0.5 mL of AB in 5 mL water (90.9 mM AB), stirring rate of 1400 rpm, and 40 °C.

2.5. Effect of AB Concentration

The effect of AB concentration on the generation of H_2 was also examined by performing experiments varying the concentration of AB and keeping constant all the other parameters. It is evident from Figure 6, that the reaction rates of 45.5 and 90.9 mM overlap during the early stages and the TOF values were similar (Figure S4). On the other hand, for the concentration of 22.7 mM the reaction seemed to proceed slower but with over 99% H_2 yield. The reason behind this is the low concentration of AB compared to the amount of catalyst. Since there was not enough reactant to take over the catalytic active sites, the reaction rate was lower. The model data are in good agreement with the experimental.

2.6. Effect of Substrate to Catalyst Ratio

The influence of the amount of catalyst was also studied. As expected, increasing the mass of catalyst decreases the reaction time (Figure 7) since more active sites are available for AB to produce H_2. However, a drop at TOF was observed at the highest ratio of 1000:1 (Figure 8), indicating that the additional catalyst amount is not effectively utilized, due to possible transfer limitations or the reaction reached its kinetic limit. Even though the

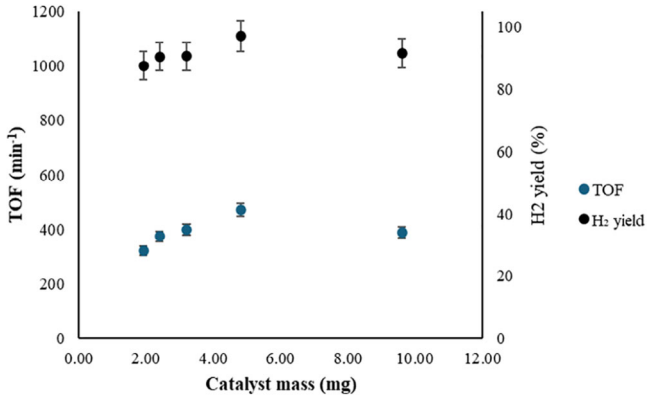

Figure 8. TOF values (left *y*-axis) and H_2 yield (right *y*-axis) at catalyst mass of 1.92–9.62 mg (5000:1–1000:1 substrate to catalyst ratio).

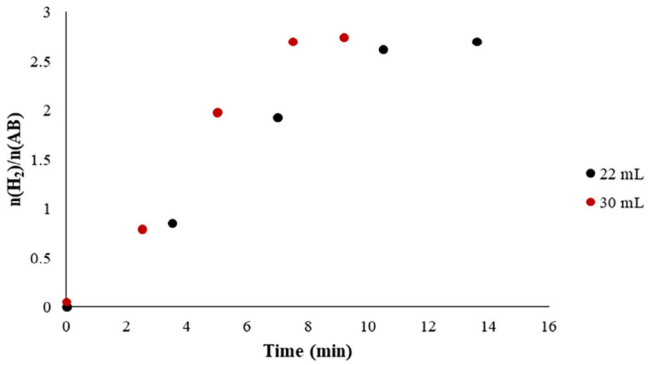

Figure 9. Effect of reactor size on AB hydrolysis. Reaction conditions: 0.5 mL of AB in 5 mL water (90.9 mM AB), stirring rate of 1400 rpm, 3000:1 substrate to metal molar ratio, and 40 °C.

ratio of 2000:1 gave the best results in terms of H_2 yield and TOF, it was not chosen as the optimum value since the 3000:1 gave similar results and by choosing the 3000:1 ratio, less amount of catalyst would be required given the necessity to perform more catalytic tests. By observing the graph, the model gave good predictions of the experimental data. However, there is slight deviation, 9% for the ratios of 3000:1 and 4000:1 and 13% for the ratio of 5000:1. Even though in reality the number of available active sites is a limiting factor for the reaction, the model does not include this, assuming that the amount of catalyst is sufficient. The influence of the support was also investigated at 40 °C, where the H_2 yield was 0% with negligible activity, showcasing that the support had no ability to catalyze the hydrolytic reaction.

2.7. Effect of Reactor Size

Two reactors were examined with similar shape of a round bottom with two necks. Their geometry allows uniform heating and stirring. One reactor was bigger with total capacity of 30 mL, while the second was smaller with a capacity of 22 mL. Both reactors achieved the same H_2 yield of 90% (Figure 9). When the reactor of 30 mL was used, the reaction was completed in less time. A study by Basu et al.,[33] on AB hydrolysis used a 25 mL batch reactor where a similar trend was observed with a ratio of 3 and a reaction time of 10 min. Thus, the reactors within the range of 20–30 mL and similar shape might not significantly influence the production of H_2, achieving a similar trend. Also, in a previous study from our group,[22] a 35 mL reactor was used for the decomposition of hydrous hydrazine, where H_2 yield was 93%, close to a ratio of 3.

2.8. Statistical Analysis

A statistical analysis is conducted here to underline the significance of the various factors, including temperature, stirring rate, AB concentration, and substrate (AB) to catalyst ratio (Sub/Cat), on the three response variables: reaction time, TOF, and H_2 yield. The objective of this statistical analysis is to rank the significance of main effects and two-factor interactions for each response variable, thereby guiding the design of future experiments aimed at further optimizing H_2 yield, achieving relatively low reaction times, and attaining high TOF by focusing exclusively on the most influential factors and their interactions, identified in this study. Moreover, statistical analysis ensures that the results from the experiments are statistically significant and not due to random variations. The influence of the reactor size is not considered into the analysis, as it is observed that the H_2 yield remained consistent irrespective of the reactor size. It is important to note that the broader scope of statistical analysis extends beyond making conclusions about the importance of individual factors. It also seeks to explore the interactions and relationships between the factors and the response variables, with the aim of developing predictive models using machine learning techniques. However, within the context of this study, the experiments were conducted using a one-factor-at-a-time (OFAT) approach, which enables the evaluation of the significant influence of each factor (main effects) only. In future work, we aim to employ more sophisticated experimental designs by using design of experiment (DoE) techniques to quantify not only the main effects but also two-factor, three-factor, and higher-order interactions for the purpose of developing effective predictive models using machine learning techniques.

Table 1 presents a summary of the experimental results concerning the response variables associated with the four factors studied here. The longest reaction time was observed when the smallest amount of catalyst was used, whereas the shortest reaction time occurred with the largest amount of catalyst, indicating a strong correlation between reaction time and catalyst amount. For TOF, the lowest values were recorded at the lowest temperature, while the highest TOF was achieved at the highest temperature, demonstrating a clear dependence of TOF on temperature. Regarding H_2 yield, a strong correlation was observed with stirring rate, where low stirring rates resulted in low hydrogen yields. Additionally, for low AB concentration, the H_2 yield, measured as a percentage rather than absolute mass, was the highest.

To ensure the robustness and validity of the ANOVA calculations presented here, key assumptions were checked thoroughly and verified prior to conducting the analyses. Quantile–Quantile

Table 1. Summary of the experimental results examining the effects of four factors on three response variables.

Temperature	Stirring	Concentration (mM)	Sub:Cat	Reaction Time (min)	TOF (min^{-1})	H_2 Yield (%)
40	1400	22.7	3000	17.11	231.35	**94.36**
40	1400	45.5	3000	9.80	370.77	90.42
40	1400	90.9	3000	8.05	402.16	86.51
40	250	90.9	3000	11.21	330.77	**80.53**
40	500	90.9	3000	10.95	429.52	93.37
40	750	90.9	3000	9.49	419.68	88.11
40	1400	90.9	3000	8.06	400.00	86.95
40	1400	90.9	5000	**18.77**	323.37	83.61
40	1400	90.9	4000	12.00	373.74	86.29
40	1400	90.9	3000	8.08	397.89	86.46
40	1400	90.9	2000	4.99	475.85	92.64
40	1400	90.9	1000	**2.71**	391.68	87.64
30	1400	90.9	3000	16.63	**201.28**	89.49
40	1400	90.9	3000	7.99	404.97	86.54
50	1400	90.9	3000	3.86	**1003.08**	90.95

(QQ) plots were used to assess whether the residuals followed a normal distribution. For reaction time and H_2 yield, normality held up well across all factors, and for TOF, temperature also met the normality assumption. However, slight departures from normality were noted for TOF under concentration, stirring, and Sub/Cat. Variance homogeneity using box plots was then examined. Temperature, stirring, and Sub/Cat levels showed consistent variance, whereas concentration displayed more variability, especially for H_2 yield, indicating a less uniform spread. QQ plots and box plots are provided in the supplementary file (Figures S5 and S6, respectively).

To explore whether changes in factor levels resulted in statistically significant differences in the means of the responses and to quantify how each factor affected these responses, one-way ANOVA was performed using the Isalos data analytics platform. The results are shown as a heat map (Figure 10), which displays the p-values for each factor-response pair, with darker colors indicating stronger statistical significance. The analysis showed a very strong influence of temperature on TOF ($p = 7.7 \times 10^{-7}$), well below $p \leq 0.05$ (the commonly used significance threshold). Although temperature influences TOF significantly, it has a minimal effect on hydrogen (H_2) yield, as shown by the high p-value of 0.73. This suggests that the hydrolytic reaction of AB appears to approach thermodynamic equilibrium under the conditions studied (ranging from 30 °C to 50 °C), thereby explaining why H_2 yield remains relatively unchanged despite the faster reaction rates. In contrast, the amount of catalyst's effect on reaction time approached the threshold of $p \leq 0.05$ ($p = 0.096$), suggesting a potential influence. The impact of stirring on H_2 yield was near-significant ($p = 0.077$), indicating a possible role in determining H_2 yield. Bar charts presenting the F-statistics derived from the one-way ANOVA are provided in the supplementary file (Figure S7). A dashed red line indicates the critical F-value corresponding to the 95% significance level ($p \leq 0.05$). The observations from the bar charts are consistent with the p-values presented in the heat map, thereby offering complementary evidence of the relative contributions of each factor. Additionally, the bar charts present the cumulative effect of each factor on the responses (blue line). The one-way ANOVA has effectively identified temperature as a critical factor influencing TOF and highlighted the effects of catalyst concentration and stirring rate in optimizing the AB hydrolytic reaction. By prioritizing these factors in future experimental designs, multifactorial experimental designs should be adopted to capture the complex interactions between these factors to achieve a more efficient and effective hydrogen production process.

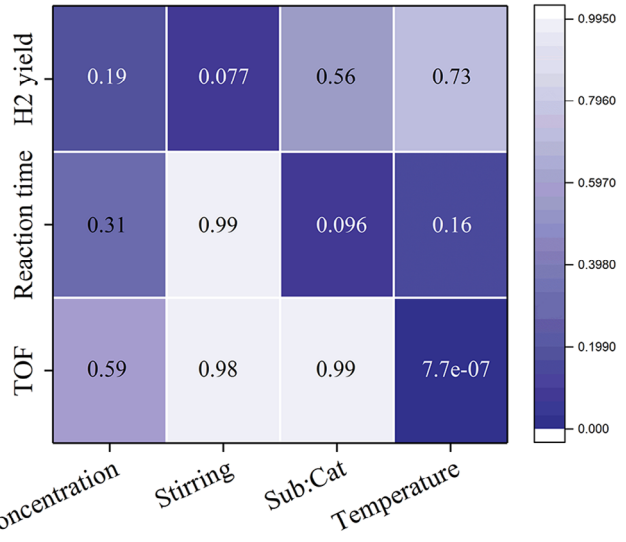

Figure 10. Heat map representation of the p-values computed from the one-way ANOVA analysis of the four factors (temperature, substrate-to-catalyst ratio, stirring, and concentration) and three response variables (TOF, reaction time, and H_2 yield).

As previously mentioned, the OFAT experimental design does not provide a high degree of accuracy in quantifying interactions between factors. Despite this limitation, to gain preliminary insights, two-factor interactions were evaluated using factorial

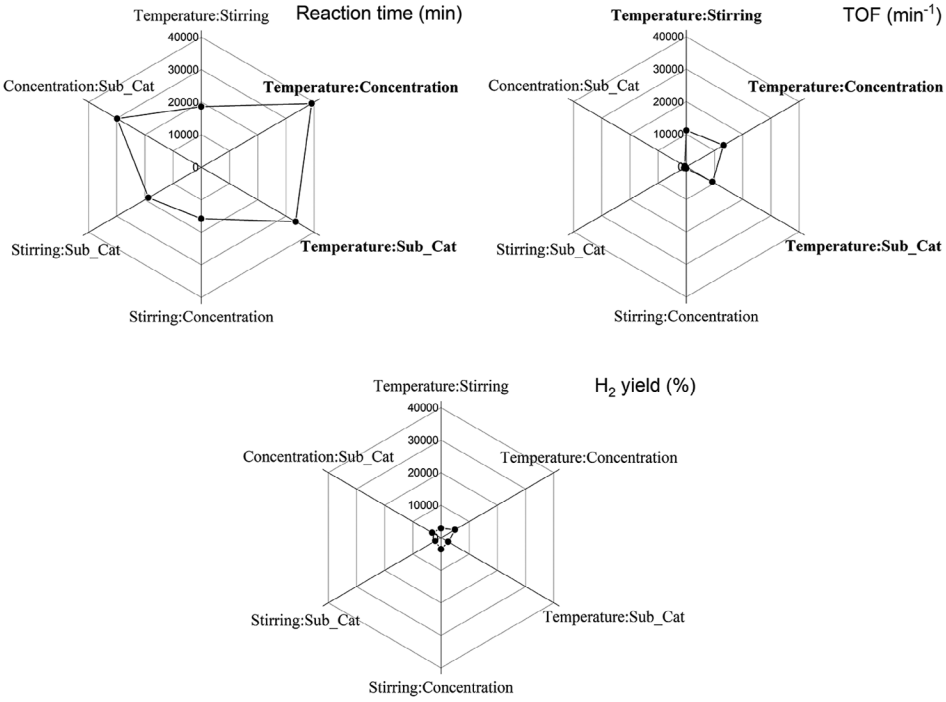

Figure 11. Radar plots illustrating the F-statistics derived from factorial ANOVA for assessing the effects of two-factor interactions on the responses.

ANOVA through the Isalos data analytics platform. Figure 11 presents radar plots of F-statistics derived from the factorial ANOVA for two-factor interactions, illustrating how each two-factor interaction influences the response variables. For the reaction time response, combining temperature with either concentration or catalyst amount had a pronounced effect. By contrast, two-factor interactions played a smaller role in TOF response, and their impact on hydrogen production yield was even less apparent. These insights highlight the critical role of temperature in optimizing reaction time and TOF, especially when combined with appropriate concentration and catalyst amount. Conversely, the minimal impact of two-factor interactions on H_2 yield suggests that maintaining optimal individual factors is sufficient to achieve high hydrogen production without the need for complex multi-factor adjustments. Future experimental designs should prioritize optimizing temperature and catalyst amount to maximize TOF and reduce reaction time, while ensuring adequate concentration to sustain high H_2 yields.

The Pearson correlation analysis was performed to quantify the strength and direction of linear relationships between the three response variables: TOF, reaction time, and H_2 yield. The results are visualized in a heat map (Figure 12), which provides a clear representation of the correlation coefficients. The Pearson correlation between TOF and reaction time was found to be −0.62, indicating a moderate negative correlation. This suggests that as reaction time decreases, TOF tends to increase, which is consistent with the expectation that faster reactions often result in higher turnover frequencies. The correlation between H_2 yield and reaction time was −0.08, indicating a very weak negative relationship. This weak correlation suggests that reaction time has little to no consistent linear influence on hydrogen yield within the experimental conditions explored. Finally, the correlation between H_2 yield and TOF was 0.18, indicating a weak positive relationship. While a slight increase in H_2 yield with higher TOF is observed, the relationship is not strong enough to suggest a significant or consistent linear dependency. Given the moderate negative correlation between TOF and reaction time, efforts to enhance TOF through temperature optimization are likely to yield more efficient catalytic performance, while the weak correlations involving H_2 yield suggest that its optimization may require independent control of factors beyond those influencing TOF and reaction time.

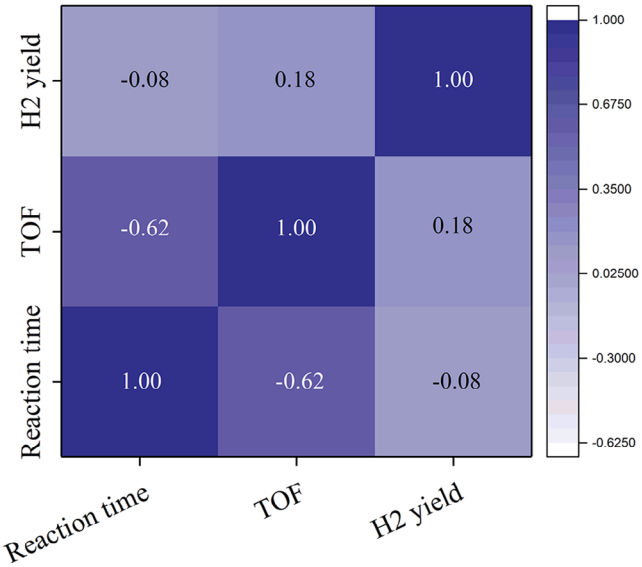

Figure 12. Heat map of Pearson correlation coefficients illustrating the linear relationships between the three response variables: TOF, reaction time, and H_2 yield.

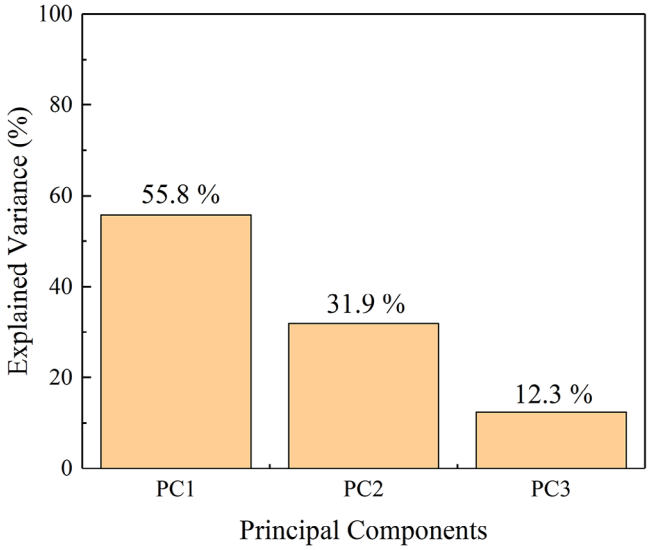

Figure 13. Variance percentage for each principal component (PC) derived from the PCA analysis.

Table 2. PCA loadings for each variable on the three principal components (PC1, PC2, and PC3).

Variable	PC1	PC2	PC3
Reaction time	−0.67	0.28	0.69
TOF	0.69	−0.10	0.71
H_2 yield	0.27	0.96	−0.12

Principal Component Analysis (PCA) was conducted to examine the variance structure among the three response variables and to identify patterns in their contributions to the principal components (PCs). The explained variance associated with each component indicates how much of the total variability in the dataset is captured by that component. PCA revealed that PC1 and PC2 together account for 87.7% of the total variance in the dataset, with PC1 explaining 55.8% and PC2 contributing 31.9% (Figure 13). The variance explained by PC3 is only 12.3%, suggesting that its contribution is minimal compared to the first two components. The low variance explained by PC3 and its insignificant loadings indicate that additional factors or higher-order interactions have a negligible impact on the response variables. Resources can be efficiently allocated by focusing on the first two principal components, which capture the majority of the system's variability, thereby streamlining the optimization process.

The variable loadings on each principal component reveal the contributions of the response variables to the respective components (Table 2). The loadings for PC1 show that reaction time, TOF, and H_2 yield contribute −0.67, 0.69, and 0.27, respectively, highlighting a contrast between reaction time and TOF with a smaller role for H_2 yield. The strong negative loading of reaction time and positive loading of TOF on PC1 indicate that reducing reaction time is closely associated with increasing TOF. This relationship underscores the critical role of temperature in enhancing catalytic performance by accelerating reaction kinetics. For PC2, the loadings are 0.28, −0.10, and 0.96, indicating that this component is dominated by H_2 yield, with weaker contributions from reaction time and TOF. Since H_2 yield is less correlated with reaction time and TOF, optimizing hydrogen production may require independent control, as already discussed. Given the minimal explained variance of PC3, its loadings (0.69, 0.71, and −0.12 for reaction time, TOF, and H_2 yield, respectively) are not considered significant for the interpretation of the data.

3. Conclusion

Concluding, in this work, the hydrolysis of AB was extensively studied, varying different parameters, such as temperature, stirring rate, AB concentration, and AB to catalyst molar ratio. Results showed over 85% H_2 yield. The highest TOF value was achieved at the highest studied temperature of 50 °C and was 1004 min^{-1}, while at 40 °C, which was the optimum temperature used in this study, the TOF value was 400 min^{-1}. The CFD studies were also in great agreement with the experimental data, validating the results with a maximum error of 13%. The effect of support was also tested, and it was noticed that when the support was used by itself at 40 °C, no H_2 was produced. Thorough statistical analyses were conducted using Isalos data analytics platform, including one-way ANOVA, factorial ANOVA, Pearson correlation, and PCA to provide a comprehensive understanding of the factors influencing the AB hydrolytic reaction's key performance indicators: TOF, reaction time, and H_2 yield. One-way ANOVA revealed that temperature has a highly significant effect on TOF ($p = 7.7 \times 10^{-7}$) but a minimal impact on H_2 yield ($p = 0.73$), suggesting that elevated temperatures accelerate reaction kinetics without substantially increasing hydrogen production due to the reaction approaching thermodynamic equilibrium. Factorial ANOVA further demonstrated that two-factor interactions, particularly between temperature and concentration or catalyst amount, significantly affect reaction time, whereas their influence on TOF and H_2 yield remains limited. Thus, future experiments will focus on the combination of these two parameters to achieve less reaction time. Pearson correlation analysis showed a moderate negative correlation between TOF and reaction time ($r = -0.62$), indicating that higher TOF is associated with shorter reaction times, while the correlations between H_2 yield and both reaction time ($r = -0.08$) and TOF ($r = 0.18$) are weak, suggesting minimal linear relationships. PCA identified that the first two principal components account for 87.7% of the total variance, with PC1 primarily associated with TOF and reaction time and PC2 dominated by H_2 yield, thereby highlighting the distinct factors influencing each response variable. Based on these findings, temperature is ranked as the most important factor for optimizing TOF, followed by stirring rate and catalyst concentration for H_2 yield, and substrate-to-catalyst ratio for reaction time. Moving forward, future research should focus on multi-factorial optimization techniques such as Response Surface Methodology (RSM) to refine experimental conditions, enhance H_2 yield, and improve overall reaction efficiency by strategically targeting the most influential factors identified through this comprehensive analysis and by combining factors such as tem-

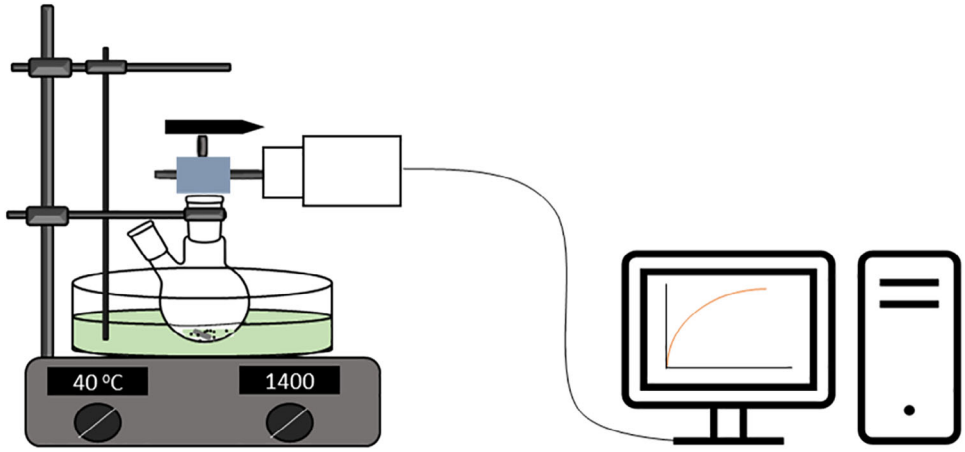

Figure 14. Schematic diagram of the experimental set-up.

perature and AB or catalyst concentration for optimization of the process. Additionally, this will enable integrating machine learning algorithms and CFD for developing predictive models to facilitate the identification of optimal operational parameters and accelerate the optimization process.

4. Experimental and Computational Section

4.1. Catalytic Hydrolysis

The catalytic experiments were conducted utilizing an $Ir/Ni_{10}Ce$ catalyst, where its synthesis and characterization are described in the Supporting Information. The reaction took place in a batch reactor of 30 mL total volume capacity on top of a magnetic stirring hot plate. The catalyst and a magnetic stirrer were added in the reactor containing 5 mL of distilled water (Figure 14). After an equilibrium of the system and when the system reached the desired temperature, the desired amount of AB was added to the reactor. The flask was connected to a gas collection system (Man On the Moon X102 kit), measuring the partial pressures of the generated H_2. Using the ideal gas law (Equation 2) the pressure of H_2 produced was quantified by calculating the moles of H_2.

$$pV = nRT \tag{2}$$

These data were then transformed into a dimensionless ratio (λ) between the number of released moles and the initial amount of AB added to the system.

$$\lambda = \frac{n\,(H_2)}{n\,(NH_3BH_3)} \tag{3}$$

The turnover frequency (TOF) values were also calculated based on Equation (4), assuming all metal particles take part in the reaction.

$$TOF = \frac{n_{NH_3BH_3\,consumed}}{3n_{metal}t} \tag{4}$$

4.2. Reaction Kinetics

Many studies[3,37,33,38–40,34,41–46] proposed that AB hydrolysis follows Langmuir–Hinshelwood kinetics since the reaction order was found between zero and one. The hydrolysis reaction rate was modeled using a simple Langmuir-Hinshelwood approach, as shown below (Equation 5), based on the assumption that AB is adsorbed in the catalytic surface and subsequently reacts to form H_2. This model gave good validation and thus, it was chosen as a suitable model for this reaction. Moreover, a study suggested that this kinetic model is suitable for temperatures up to 60 °C,[34] which was within the temperature range of this work (30–50 °C).

$$r = \frac{kK_{ads.}C_{AB}}{1 + (K_{ads.}C_{AB})} \tag{5}$$

In the equation above, r represents the rate expression ($mol/m^3.s$), k is the specific rate constant ($mol/m^3.s$), K_{ads} is the Langmuir adsorption equilibrium constant (m^3/mol), and C_{AB} denotes the initial concentration of AB (mol/m^3).

4.3. Batch Reactor Modeling

Since the experiments were carried out in a batch reactor, which is ideally mixed (no inflow or outflow), a zero-dimensional (0D) model was developed utilizing the COMSOL v6.0 simulation software, based on the assumptions of constant volume and ideal fluids. The feature Reaction Engineering was used, incorporating the mass balance (Equation 6) for each component, i, considering constant volume.

$$\frac{dc_i}{dt} = R_i \tag{6}$$

In the above equation, c_i is the concentration for each specie, i, (mol/m^3), t is the time (s) and R_i denotes the sum of each components rate expression ($mol/m^3.s$).

Along with Equation (6), the reaction rate (Equation 5) was implemented in COMSOL v6.0 for the validation of the experi-

mental data. The CFD evaluated parameters were temperature, stirring rate, AB concentration, and AB to catalyst molar ratio. The batch system had 4 degrees of freedom and an average of 7 s of computational time. A table (Table S2) with the modelling parameters is presented in the Supporting Information.

4.4. Statistical Analysis

Comprehensive statistical analyses were conducted using the Isalos data analytics platform,[47,48] employing analysis of variance (ANOVA) and principal component analysis (PCA) to evaluate the efficiency of the hydrolytic reaction of AB investigated in this study. In general, thorough statistical analysis has not been implemented for catalytic H_2 production processes, therefore, this analysis will bring foremost statistical important parameters that influence H_2 yield in the hydrolytic reaction of AB. Specifically, the main effects and interactions of temperature, stirring rate, AB concentration, and substrate (AB) to catalyst ratio (Sub/Cat) were assessed with respect to the three response variables: reaction time, TOF and H_2 yield. ANOVA and PCA were employed in this study with the objective of ranking the relative importance of each main factor and two-factor interactions for each response variable. A clear relationship between the measured signals (factors) and certain groups of observations (response variables) was established to address the significance of each factor in relation to each response variable. This, along with the experimental results, will refine future experimentation, enabling a focused and detailed investigation of the factors identified as critical, thereby optimizing the hydrolytic reaction of AB for maximizing the hydrogen yield, minimizing reaction times, and achieving high TOF. The combination of ANOVA and PCA has been widely used to optimize chemical reactions in various chemical engineering processes,[49] including biodiesel production,[50] syngas generation[51] and the synthesis of *n*-benzylideneaniline.[52]

Quantile-Quantile (QQ) plots were generated for each factor-response pair to assess the normality of residuals, a critical assumption for subsequent parametric tests. For a given response variable *Y* and factor *F*, a one-way Analysis of Variance (ANOVA) model is fitted as.[53]

$$Y_{ij} = \mu + \alpha_i + \varepsilon_{ij} \tag{7}$$

where Y_{ij} denotes the *j*-th observation of *Y* at the *i*-th level of *F*, μ represents the overall mean, α_i is the effect of the *i* -th factor level, and $\boldsymbol{\varepsilon_{ij}}$ is the residual (random) error associated with Y_{ij} assumed to follow a normal distribution. The residuals ε_{ij} are ordered and plotted against theoretical quantiles.

$$z_i = \Phi^{-1}\left(\frac{i - 0.5}{n}\right) \tag{8}$$

where Φ^{-1} is the inverse cumulative distribution function of the standard normal distribution, and *n* is the total number of residuals. A linear alignment of points in the QQ plot indicates that the residuals follow the normal distribution, thereby validating the subsequent use of parametric ANOVA tests.

Box plots were used to visualize the distribution, central tendency, and variability of responses across factor levels. For each group (corresponding to a specific factor level), statistical measures such as the median (Q_2), first quartile (Q_1), third quartile (Q_3) and interquartile range (IQR = Q_3–Q_1) are calculated to generate box plots.[54]

One-way ANOVA was used to test for significant differences in group means, allowing for the quantification of the main effects of individual factors: temperature, stirring rate, AB concentration, and substrate (AB) to catalyst ratio (Sub/Cat) on responses: reaction time, TOF and H_2 yield. The total variability in *Y* is partitioned into between-group sum of squares as.[55]

$$SS_{Between} = \sum_{i=1}^{k} n_i\left(\bar{Y}_i - \bar{Y}\right)^2 \tag{9}$$

within group sum of squares as.

$$SS_{Within} = \sum_{i=1}^{k}\sum_{j=1}^{n_i}\left(Y_{ij} - \bar{Y}_i\right)^2 \tag{10}$$

and total sum of squares as.

$$SS_{Total} = SS_{Between} + SS_{Within} \tag{11}$$

where *k* represents the number of factor levels, n_i the number of observations in group *i*, $\bar{Y}_i$ the mean of group *i*, and $\bar{Y}$ the overall mean. The degrees of freedom associated with these sums are calculated as $df_{Between} = k - 1$, $df_{Within} = N - k$ (where *N* is the total number of observations, $N = \sum_{i=1}^{k} n_i$) and $df_{Total} = N - 1$. The mean squares are then derived as.

$$MS_{Between} = \frac{SS_{Between}}{df_{Between}} \tag{12}$$

$$MS_{Between} = \frac{SS_{Between}}{df_{Between}} \tag{13}$$

leading to the computation of the F-statistic as.

$$F = \frac{MS_{Between}}{MS_{Within}} \tag{14}$$

The p-value is calculated using the cumulative distribution function (CDF) of F-distribution, which is parametrized by the degrees of freedom df_1 (numerator) and df_2 (denominator), given by.

$$p - value = P\left(F_{df1,df2} \geq F\right) \tag{15}$$

where *F* is the observed F-statistic and $F_{df1,df2}$ represents the F-distribution with df_1 and df_2 degrees of freedom. A p-value less than or equal to the significance level (commonly $\alpha = 0.05$) indicates that there are statistically significant differences between the group means.

This was further extended by factorial ANOVA, which examines the simultaneous influence of multiple factors and their interactions, providing deeper insights into complex dependencies. For each pair of factors, a two-way ANOVA model is

specified as.

$$Y_{ijk} = \mu + \alpha_i + \beta_j + (\alpha\beta)_{ij} + \varepsilon_{ijk} \quad (16)$$

where Y_{ijk} is the *k*-th observation at the *i*-th level of factor F_a and the *j*-th level of factor F_b, α_i and β_j represent the main effects of factors F_a and F_b, respectively. The term $(\alpha\beta)_{ij}$ captures the interaction effect between the two factors and ε_{ijk} is the residual error. The interaction effects are quantified through F-statistics as.

$$F_{(\alpha\beta)} = \frac{MS_{(\alpha\beta)}}{MS_E} \quad (17)$$

where $MS_{(\alpha\beta)}$ is the mean square for the interaction effect and MS_E is the mean square error from the ANOVA table.

To explore the linear relationships among the response variables, Pearson correlation analysis was conducted. The Pearson correlation coefficient r_{YZ} between any two response variables *Y* and *Z* is calculated using the formula.[56]

$$r_{YZ} = \frac{\sum_{i=1}^{n}\left(Y_i - \bar{Y}\right)\left(Z_i - \bar{Z}\right)}{\sqrt{\sum_{i=1}^{n}\left(Y_i - \bar{Y}\right)^2}\sqrt{\sum_{i=1}^{n}\left(Z_i - \bar{Z}\right)^2}} \quad (18)$$

where Y_i and Z_i are individual observations of *Y* and *Z* and $\bar{Y}$ and $\bar{Z}$ are the means of *Y* and *Z*. The term *n* is the total number of observations. The resulting correlation coefficients range from -1 to $+1$ indicating strong positive or negative correlations.

Last, principal component analysis (PCA) was performed to examine the variance structure among the three response variables: reaction time, TOF and H_2 yield and to identify patterns in their contributions to the principal components (PCs). By focusing on the principal components that account for most of the variance, the study could prioritize factors that have the most substantial impact on AB hydrolytic reaction, thereby enabling more effective and strategic experimental designs. The data matrix *X*, comprising the centered response variables, is constructed by subtracting the mean of each variable from the corresponding data points.[57]

$$X_{centered} = X - 1_n \bar{X} \quad (19)$$

where *X* is the original data matrix of size *n* x *p*, with $p = 3$ representing the response variables, 1_n is an *n* x 1 vector of ones and $\bar{X}$ is a 1 x *p* vector of column means. The covariance matrix Σ is then calculated as.

$$\Sigma = \frac{1}{n-1} X_{centered}^{T} X_{centered} \quad (20)$$

Subsequent eigen-decomposition of Σ yields the eigenvectors matrix *V* and the diagonal matrix of eigenvalues Λ, ordered in descending magnitude. The principal component scores *Z* are obtained via.

$$Z = X_{centered} V \quad (21)$$

The proportion of variance explained by each principal component PC_k is determined using.

$$\text{Variance Percentage of } PC_k = \left(\frac{\lambda_k}{\sum_{m=1}^{p}\lambda_m}\right) \times 100\% \quad (22)$$

Author Contributions

Panayiota Adamou: Writing—original draft; investigation; methodology; formal analysis; validation; and visualization. **Eleana Harkou**: Investigation; formal analysis; validation; and visualization. **Silvio Bellomi**: Investigation; formal analysis; and validation. **Ilaria Barlocco**: Investigation and formal analysis. **Dimitris Mintis**: Writing—original draft; investigation; methodology; and formal analysis. **Antreas Afantitis**: Investigation; methodology; and formal analysis. **Juan J. Delgado**: Investigation; formal analysis; writing—review; and editing. **Xiaowei Chen**: Investigation; formal analysis; writing—review, and editing. **George Manos**: Writing—review; and editing. **Nikolaos Dimitratos**: Conceptualization; writing—review; and Editing; **Alberto Villa**: Conceptualization; writing—review; editing; and supervision. **Achilleas Constantinou**: Conceptualization; writing—review; editing; and supervision.

Acknowledgements

Open access publishing facilitated by Universita degli Studi di Milano, as part of the Wiley - CRUI-CARE agreement.

Conflict of Interests

The authors declare no conflict of interest.

Data Availability Statement

The data that support the findings of this study are available from the corresponding author upon reasonable request.

Keywords: Ammonia borane · Hydrogen · Hydrolysis · Modelling · Statistical analysis

[1] S. Singh, S. Jain, V. Ps, A. K. Tiwari, M. R. Nouni, J. K. Pandey, S. Goel, *Renew. Sustain. Energy Rev.* **2015**, *51*, 623–633.
[2] C. Lang, Y. Jia, X. Yao, *Energy Storage Mater.* **2020**, *26*, 290–312.
[3] S. Basu, Y. Zheng, A. Varma, W. N. Delgass, J. P. Gore, *J. Power Sources* **2010**, *195*, 1957–1963.
[4] U. Sanyal, U. B. Demirci, B. R. Jagirdar, P. Miele, *ChemSusChem* **2011**, *4*, 1731–1739.
[5] S. Akbayrak, S. Özkar, *Int. J. Hydrog. Energy* **2018**, *43*, 18592–18606.
[6] Q. Xu, M. Chandra, *J. Power Sources* **2006**, *163*, 364–370.
[7] J. Hu, Z. Chen, M. Li, X. Zhou, H. Lu, *ACS Appl. Mater. Interfaces* **2014**, *6*, 13191–13200.
[8] K. Mori, K. Miyawaki, H. Yamashita, *ACS Catal.* **2016**, *6*, 3128–3135.
[9] L.-T. Guo, Y.-Y. Cai, J.-M. Ge, Y.-N. Zhang, L.-H. Gong, X.-H. Li, K.-X. Wang, Q.-Z. Ren, J. Su, J.-S. Chen, *ACS Catal.* **2015**, *5*, 388–392.

[10] K. Guo, H. Li, Z. Yu, *ACS Appl. Mater. Interfaces* **2018**, *10*, 517–525.
[11] F. Fu, C. Wang, Q. Wang, A. M. Martinez-Villacorta, A. Escobar, H. Chong, X. Wang, S. Moya, L. Salmon, E. Fouquet, J. Ruiz, D. Astruc, *J. Am. Chem. Soc.* **2018**, *140*, 10034–10042.
[12] M. Chandra, Q. Xu, *J. Power Sources* **2006**, *156*, 190–194.
[13] K. Yao, C. Zhao, N. Wang, T. Li, W. Lu, J. Wang, *Nanoscale* **2020**, *12*, 638–647.
[14] M. Shingole, S. Banerjee, P. Ruz, A. Kumar, P. Sharma, V. Sudarsan, *Catal. Sci. Technol.* **2024**, *14*, 6338–6350.
[15] C. Yüksel Alpaydın, S. K. Gülbay, C. Ozgur Colpan, *Int. J. Hydrog. Energy* **2020**, *45*, 3414–3434.
[16] X. Li, C. Zeng, G. Fan, *Int. J. Hydrog. Energy* **2015**, *40*, 3883–3891.
[17] S. Hafeez, F. Sanchez, S. M. Al-Salem, A. Villa, G. Manos, N. Dimitratos, A. Constantinou, *Catalysts* **2021**, *11*, 341.
[18] A. I. Tsiotsias, N. D. Charisiou, E. Harkou, S. Hafeez, G. Manos, A. Constantinou, A. G. S. Hussien, A. A. Dabbawala, V. Sebastian, S. J. Hinder, M. A. Baker, K. Polychronopoulou, M. A. Goula, *Appl. Catal. B Environ.* **2022**, *318*, 121836.
[19] S. Hafeez, S. M. Al-Salem, A. Bansode, A. Villa, N. Dimitratos, G. Manos, A. Constantinou, *Ind. Eng. Chem. Res.* **2022**, *61*, 1655–1665.
[20] S. Hafeez, E. Harkou, P. Adamou, I. Barlocco, E. Zanella, G. Manos, S. M. Al-Salem, X. Chen, J. J. Delgado, N. Dimitratos, A. Villa, A. Constantinou, *Nanomaterials* **2023**, *13*, 2993.
[21] E. Harkou, P. Adamou, K. Georgiou, S. Hafeez, S. M. Al-Salem, A. Villa, G. Manos, N. Dimitratos, A. Constantinou, *Molecules* **2023**, *28*, 5399.
[22] P. Adamou, S. Bellomi, E. Harkou, X. Chen, J. J. Delgado, N. Dimitratos, G. Manos, A. Villa, A. Constantinou, *Chem. Eng. J.* **2024**, *493*, 152715.
[23] A. I. Tsiotsias, E. Harkou, N. D. Charisiou, V. Sebastian, D. R. Naikwadi, B. van der Linden, A. Bansode, D. Stoian, G. Manos, A. Constantinou, M. A. Goula, *J. Energy Chem.* **2024**, *102*, 309–328. https://doi.org/10.1016/j.jechem.2024.11.001.
[24] E. Harkou, S. Hafeez, G. Manos, A. Constantinou, *Processes* **2021**, *9*, 1515.
[25] E. Harkou, S. Hafeez, P. Adamou, Z. Zhang, A. I. Tsiotsias, N. D. Charisiou, M. A. Goula, S. M. Al-Salem, G. Manos, A. Constantinou, *Environ. Res.* **2023**, *236*, 116760.
[26] J. Mandel, *The Statistical Analysis of Experimental Data*, Dover Publication, New York, **1964**.
[27] M. C. Denney, V. Pons, T. J. Hebden, D. M. Heinekey, K. I. Goldberg, *J. Am. Chem. Soc.* **2006**, *128*, 12048–12049.
[28] A. Paul, C. B. Musgrave, *Angew. Chem., Int. Ed.* **2007**, *46*, 8153–8156.
[29] G. C. Fortman, A. M. Z. Slawin, S. P. Nolan, *Organometallics* **2011**, *30*, 5487–5492.
[30] D. J. Nelson, B. J. Truscott, J. D. Egbert, S. P. Nolan, *Organometallics* **2013**, *32*, 3769–3772.
[31] W.-H. Wang, H.-P. Tang, W.-D. Lu, Y. Li, M. Bao, Y. Himeda, *ChemCatChem* **2017**, *9*, 3191–3196.
[32] I. Ortega-Lepe, A. Rossin, P. Sánchez, L. L. Santos, N. Rendón, E. Álvarez, J. López-Serrano, A. Suárez, *Inorg. Chem.* **2021**, *60*, 18490–18502.
[33] S. Basu, A. Brockman, P. Gagare, Y. Zheng, P. V. Ramachandran, W. N. Delgass, J. P. Gore, *J. Power Sources* **2009**, *188*, 238–243.
[34] A. Kantürk Figen, M. B. Pişkin, B. Coşkuner, V. İmamoğlu, *Int. J. Hydrog. Energy* **2013**, *38*, 16215–16228.
[35] D. Sun, V. Mazumder, Ö. Metin, S. Sun, *ACS Nano* **2011**, *5*, 6458–6464.
[36] H. Wu, Y. Cheng, Y. Fan, X. Lu, L. Li, B. Liu, B. Li, S. Lu, *Int. J. Hydrog. Energy* **2020**, *45*, 30325–30340.
[37] S. Basu, Y. Zheng, J. P. Gore, *Am. Soc. Mech. Eng. Digital Collect.* **2009**, pp. 699–708.
[38] A. Brockman, Y. Zheng, J. Gore, *Int. J. Hydrog. Energy* **2010**, *35*, 7350–7356.
[39] J. Hannauer, U. B. Demirci, C. Geantet, J. M. Herrmann, P. Miele, *Phys. Chem. Chem. Phys.* **2011**, *13*, 3809.
[40] G. P. Rachiero, U. B. Demirci, P. Miele, *Catal. Today* **2011**, *170*, 85–92.
[41] B. C. Filiz, S. Pişkin, *Sigma J. Eng. Nat. Sci.* **2016**, *34*, 159–173.
[42] W. Chen, D. Li, Z. Wang, G. Qian, Z. Sui, X. Duan, X. Zhou, I. Yeboah, D. Chen, *AIChE J.* **2017**, *63*, 60–65.
[43] B. Coşkuner Filiz, A. Kantürk Figen, *Kinet. Catal.* **2019**, *60*, 37–43.
[44] A. M. Al-Enizi, A. Yousef, M. Ubaidullah, A. Karim, M. M. El-Halwany, *J. King Saud Univ. – Sci.* **2023**, *35*, 102538.
[45] B. Coşkuner Filiz, A. Kantürk Figen, *Int. J. Hydrog. Energy* **2023**, *48*, 22954–22966.
[46] N. Ya Dyankova, N. V. Lapin, V. V. Grinko, A. F. Vyatkin, *J. Surf. Investig. X-Ray Synchrotron Neutron Tech.* **2023**, *17*, 1001–1008.
[47] A. G. Papadiamantis, A. Afantitis, A. Tsoumanis, E. Valsami-Jones, I. Lynch, G. Melagraki, *NanoImpact* **2021**, *22*, 100308.
[48] D.-D. Varsou, A. Tsoumanis, A. G. Papadiamantis, G. Melagraki, A. Afantitis, in *Mach. Learn. Deep Learn. Comput. Toxicol.* (Ed: H. Hong), Springer International Publishing, Cham **2023**, 223–242.
[49] C. Bertinetto, J. Engel, J. Jansen, *Anal. Chim. Acta X* **2020**, *6*, 100061.
[50] F. Ferella, G. Mazziotti Di Celso, I. De Michelis, V. Stanisci, F. Vegliò, *Fuel* **2010**, *89*, 36–42.
[51] J. Yang, L. Ma, D. Zheng, S. Zhao, Y. Peng, *Energy Fuels* **2018**, *32*, 7857–7867.
[52] R. Verma, N. P. Lamba, A. Dandia, A. Srivastava, K. Modi, M. S. Chauhan, J. Prasad, *Sci. Rep.* **2022**, *12*, 9636.
[53] J. W. Osborne, Best Practices in Quantitative Methods, SAGE **2008**.
[54] C. Davino, M. Furno, D. Vistocco, *Quantile Regression: Theory and Applications*, Wiley, New York, **2013**.
[55] R. Fisher, *J. R. Stat. Soc. Ser. B Methodol.* **1955**, *17*, 69–78.
[56] K. Pearson, O. M. F. E. Henrici, *Philos. Trans. R. Soc. Lond. Ser. Contain. Pap. Math. Phys. Character* **1997**, *187*, 253–318.
[57] H. Abdi, L. J. Williams, *WIREs Comput. Stat.* **2010**, *2*, 433–459.

Manuscript received: April 3, 2025
Revised manuscript received: May 9, 2025
Accepted manuscript online: May 12, 2025
Version of record online: May 31, 2025